ELSEVIER

Tectonophysics 289 (1998) 189–201

TECTONOPHYSICS

A method to allow temporal variation of velocity in travel-time tomography using microearthquakes induced during hydraulic fracturing

Michael Fehler [a,*], Leigh House [a], W. Scott Phillips [a,1], Robert Potter [a]

[a] *Geological Engineering Group, Los Alamos National Laboratory, Los Alamos, NM 87545, USA*

Received 10 December 1996; accepted 8 July 1997

Abstract

Hydraulic injections produce fluid-filled fractures that reduce the seismic velocity of the rock compared to intact rock. The travel times of microearthquakes induced by the injections may be used to discern changes in the rock velocities, as well as locating the microearthquakes. Determining the volumes of rock where the velocities have changed provides indirect evidence for the location of the injected fluid, and the character of the changes produced in the fractured rock. Available data are generally insufficient to resolve both the spatial and temporal changes within the rock. To extract information about temporal changes, and to obtain an improved image of the velocity structure, we chose a parameterization scheme in which the velocities of each block are allowed to change from the background velocity only after a threshold number of microearthquakes have occurred in the block. Regularizing by constraining the velocity of all the altered blocks to be similar helps stabilize the inversion. The regularization can be relaxed somewhat to allow the velocity of an altered block to be different from other altered blocks if the travel-time data are compelling. The parameterization scheme is justified since observations show that the volume of the seismically stimulated rock increases linearly with the volume of the injected fluid. We applied the method to data collected in a region of Precambrian crystalline rock that was injected with 21,600 m^3 of water. We use travel times from a total of 3886 microearthquakes that were induced by the injection. The mean RMS travel-time residual decreases about 7%. The velocity structure contains a low-velocity zone located near the injection region. Other distinct low-velocity zones are identified. The pattern of microearthquake locations found using our method appears to contain more structure than the pattern found in locations determined using a homogeneous velocity structure. Two clear low-velocity regions found near the point where water was injected into the rock are separated by a region whose velocity did not change. The region of unaltered velocity had a large number of microearthquakes.

Keywords: seismic methods; seismic studies; tomography; geothermal energy; induced earthquakes

* Corresponding author. Tel.: +1 (505) 667-1925; Fax: +1 (505) 667-8487; E-mail: fehler@lanl.gov

[1] Present address: Geophysics Group, Los Alamos National Laboratory, Los Alamos, NM 87545, USA.

0040-1951/98/$19.00
PII S0040-1951(97)00315-6

1. Introduction

Travel-time tomography has provided a tool for seismologists to study earth structure and relate structure to tectonic processes (Michelini and McEvilly, 1991; Weiland et al., 1995). In addition, it has been used for characterizing smaller regions of the earth for enhancing petroleum production and extraction of geothermal energy (Nolet, 1987; Block et al., 1994). Tomographic studies are conducted using both active and passive sources. In most studies, it is reasonable to assume that the seismic structure does not change during the time that the data are collected. Block et al. (1994) analyzed travel times of microearthquakes induced by hydraulic fracturing used to generate a fracture system for a man-made geothermal energy system known as Hot Dry Rock (Harlow and Pracht, 1972). The injection of water during hydraulic fracturing introduces fractures in the rock so the velocity structure changes during the injection process. Cross-hole seismic surveys have been conducted multiple times during production from petroleum reservoirs and time-lapse tomograms have been constructed from the data to investigate the changes in the reservoir accompanying production (Paulsson et al., 1992). In this case, each tomogram can be considered as a snap-shot of the structure at the time the data were collected.

In the hydraulic fracturing study of Block et al. (1994), water was pumped into impermeable crystalline rock under high pressure for a period of 61 hours (House, 1987). Thousands of seismic events were detected by a network of borehole seismometers and located using travel times at the sensors (House, 1987; Fehler, 1989; Phillips et al., 1997). The locations of the seismic events changed with time and subsequent hydraulic measurements indicated that the permeability of the rock mass had been substantially altered by the injections (Duchane, 1994). Study of cross-well waveforms collected at depths shallower than the region studied by Block et al. (1994) indicated that the waveform character and velocity had been changed considerably by the injection of water and subsequent heat extraction (Fehler, 1981; Pearson et al., 1983; Aki et al., 1982). To increase our understanding of the hydraulic fracturing process and to aid in production of energy from Hot Dry Rock geothermal energy reservoirs, it is of interest to understand the temporal change in the physical properties of a rock mass undergoing hydraulic fracturing and heat extraction.

An initial attempt to characterize the spatial variation in the changes in physical properties of a rock mass undergoing hydraulic fracturing was made by Block et al. (1994), who analyzed travel times from induced microearthquakes at the Hot Dry Rock geothermal energy site at Fenton Hill, New Mexico, USA. A tomographic technique was used whereby locations of microearthquakes and three-dimensional velocity structure were simultaneously determined from the travel-time data. To minimize possible temporal variations in seismic structure, which was not accounted for in the inversion, a set of microearthquakes that occurred during a short time-period was chosen. When the study of Block et al. (1994) was initiated, it was anticipated that temporal variations in structure could be investigated by selecting several sets of events that occurred during distinct time-periods and constructing separate tomograms for each time-period. During the study, it was found that the changing positions of events in space and time made it difficult to compare images using data taken from different time-periods since the resolution of each image changed as the distribution of event locations used to construct the image changed.

In this study, we extend the study of Block et al. (1994) by allowing the seismic velocity structure of the reservoir to change with time. We use the simple assumption that velocity in a region stays at the background velocity until a given number of earthquakes have occurred in that region. After the number of earthquakes reaches the given number, the velocity is allowed to change but the change is restricted by the condition that all regions undergoing change should have the same velocity unless these data strongly indicate otherwise. This assumption allows us to include data from microearthquakes that occur throughout the 61 h time-period during which water was injected into the rock.

2. Data

Data were collected during a hydraulic injection into Precambrian crystalline rock at a depth of 3463 m at the Fenton Hill, USA, Hot Dry Rock geothermal energy site. A total of four borehole seismometers

were used to monitor the 61 h of water injection as well as a time-period following the injection (House, 1987). Station locations and data quality are discussed by House (1987). Fig. 1a shows the station geometry and the location of the point where water was injected into the formation. All the stations are in boreholes with two stations, EE-1 and EE-3, located near the depth of the injection interval. Station GT-1 was located some distance from the injection zone but its location in intact Precambrian crystalline rock provided high-quality seismograms. Two of the stations, EE-1 and EE-3, were three-component stations, which allowed for relatively reliable picking of S-wave arrivals. During the injection, a total of 21,600 m^3 of water was injected at a rate averaging 0.1 m^3/s (Fehler, 1989). Surface injection pressure averaged about 48 MPa.

The reservoir rock is crystalline rock of Precambrian age. The rock has undergone numerous episodes of intrusion and alteration, the most recent being caused by volcanic activities of the Jemez Volcanic field whose center is located about 20 km from the site of our investigation.

Seismic data were recorded on analog tape at the injection site and later digitized at 5000 samples/s for analysis. A total of 11,366 events were located using P- and S-arrival times from the four seismic stations. Arrival times were manually picked on a computer screen. Since frequencies were higher on seismograms from nearby stations EE-1 and EE-3, picking uncertainty was smaller at those stations. We estimate that P- and S-wave arrival times are reliable to about 1.5 ms and 2.5 ms, respectively, at these two stations. P-arrival-time uncertainties at GT-1 and

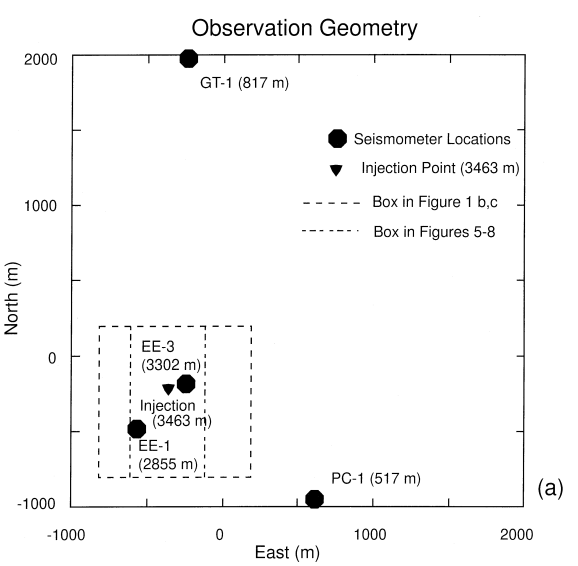

Fig. 1. (a) Plan view showing locations of seismic stations used to monitor the injection and the location of the injection. Depths in m below the surface of each station are listed beside station names. Regions plotted in more detail in (b) and (c) and Figs. 5–8 are outlined by boxes.

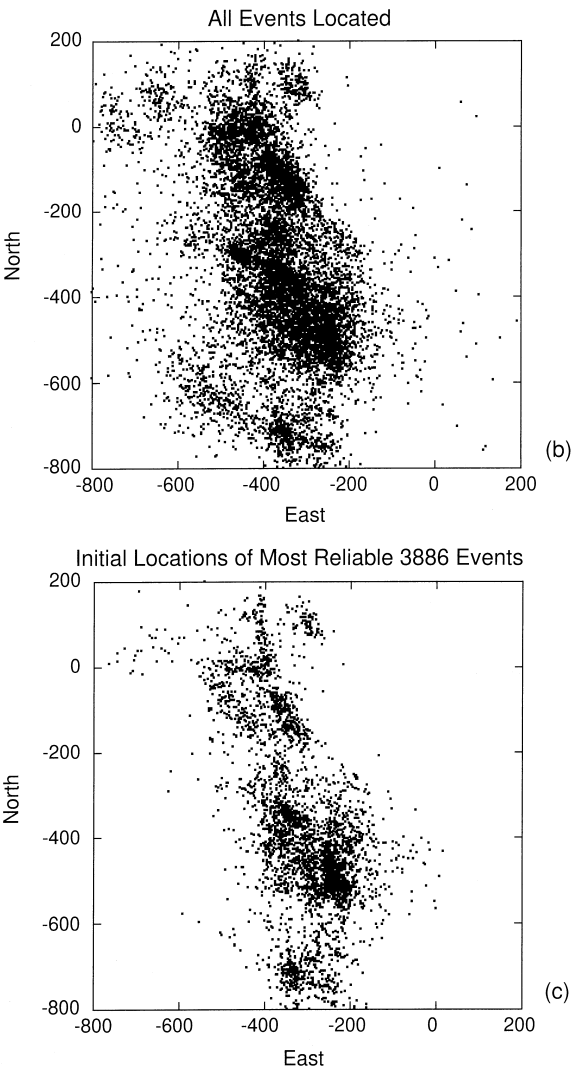

Fig. 1 (continued). (b) Plan view of all events located using homogeneous velocity model. Note difference of scale from (a). (c) Plan view map showing locations of 3886 events in (b) that are considered to be the most reliably determined.

PC-1 were estimated to be 2 ms and uncertainty in S-times at GT-1 are estimated to be 4 ms. We were not able to pick S-waves reliably at PC-1 so we did not use S-wave times from that station. Initial locations were determined using a homogeneous velocity model having P- and S-velocities of 5.92 and 3.50 km/s, respectively (House, 1987). Events occurred within about 800 m of the 20-m-long open-hole injection interval in the injection wellbore, which was centered at a depth of 3463 m below the surface. Fig. 1b shows a map view of the locations of the events. Fig. 1c shows locations of a subset of events whose locations are considered to be most reliable (discussed below).

2.1. Observations made from location data set

Fig. 2 shows the temporal change in event distances from the center of the injection interval. Although the seismic network was in operation from the beginning of the injection, no locatable events were detected during the first 5 h of injection. There are no locations for the time-period between about 30–40 h after the initiation of injection. During this time, only three stations were in operation and we chose not to analyze data from this time-period. A curve fit to the maximum distance of a majority of the seismicity vs. time is shown as the dashed line in Fig. 2. For simplicity, consider that the volume of rock that is seismically active is spherical with radius D equal to the distance from the injection zone to the furthest microearthquake from the injection zone. For the curve shown in Fig. 2, we get:

$$V_s = 4\pi D^3/3 \approx 9 \times 10^6 t = 4.5 \times 10^4 V_{inj}$$

where V_s is the seismically active volume in m^3, t is time measured in hours from the beginning of injection, and V_{inj} is the total injected fluid volume in m^3. We have taken the rate of fluid injection to be equal to the average injection rate for the 61 h of injection, which is 0.1 m^3/s.

To get a more reliable measure of the volume

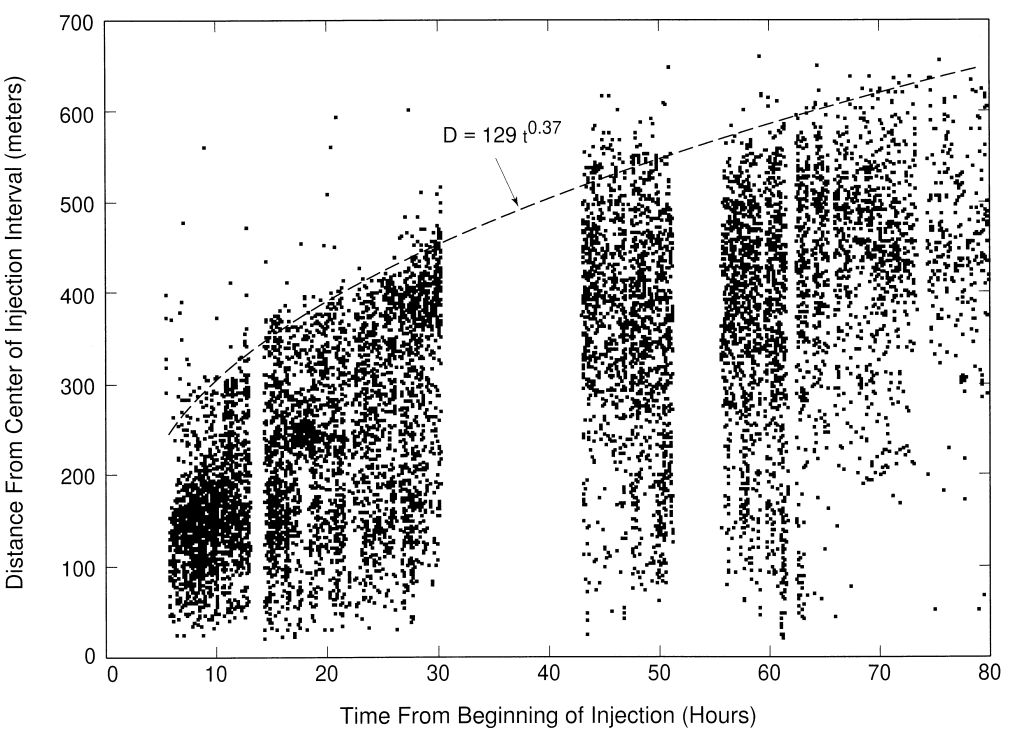

Fig. 2. Distance from center of injection zone to microearthquake location as a function of time from the beginning of injection. Results for all events shown in Fig. 1b are plotted. Line across upper portion of data is empirically determined fit to maximum distance between injection zone and microearthquake locations vs. time.

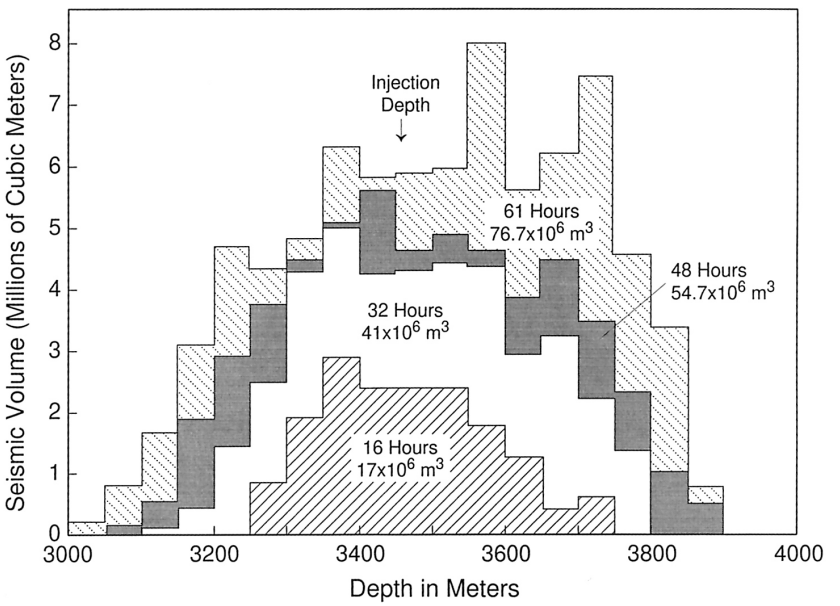

Fig. 3. Volume of seismically active region vs. depth measured from plan-view plots of microearthquake locations within 50 m depth intervals. Volume was determined for four time-periods during the injection process.

of the seismically active region, we made maps of the event distribution within 50-m-thick horizontal slabs of the seismic zone. The area of the active region within each slab was estimated by drawing a boundary around the active region and measuring the area within the boundary. The boundary was drawn so that there were holes within the seismically active region if an aseismic zone was surrounded by a seismically active zone. The volume of the seismically active region was measured using this procedure for four time intervals during the injection. Fig. 3 shows the measured volumes as a function of depth for the four intervals. Fig. 4 shows that the seismically active volume increased linearly with the injected fluid volume as $V_s = 3.33 \times 10^6 + 3.38 \times 10^3 V_{inj}$. The seismic volume calculated for the total injected fluid volume (21,600 m^3) is 76×10^6 m^3, whereas the seismic volume calculated by assuming the region is spherical is 972×10^6 m^3. The more than 10-fold disparity shows that we cannot consider the entire spherical region around the injection zone to be seismically active. It also raises concerns about the assumption that a spherical region experiences a change in velocity. The ratio of injected fluid volume to seismically active volume measured from Fig. 4 is 0.0003, which can be considered to be an effective porosity of the rock resulting from the injection, since the initial porosity of the rock is nearly zero (Trice and Warren, 1977). Figs. 2–4 show that the volume of seismically active region increases ap-

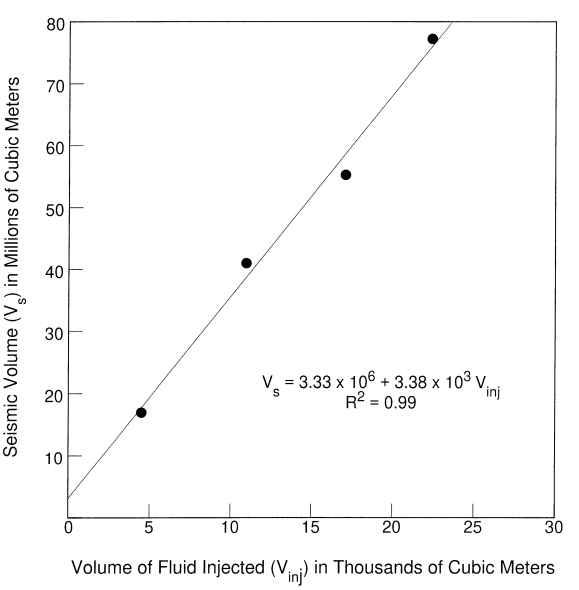

Fig. 4. Volume of seismically active region plotted in Fig. 3 vs. total injected fluid volume up to time that seismicity occurred.

proximately linearly with the injected fluid volume. We may conclude that on average, for large volumes, rock absorbs approximately the same amount of fluid over some time-period after the fluid front reaches it no matter where in the reservoir it is located.

A basic assumption in most tomography studies using earthquakes is that the velocity structure does not change over the time-period that the earthquakes occurred. Block et al. (1994) conducted their tomography study using the portion of the events shown in Fig. 1b that occurred during the 11th to 19th hour after injection began. They chose events with more than six high-quality arrival-time picks. These criteria gave them a total of 680 events for their analysis, which was considered to be a reasonable number of events to represent the seismicity during the time interval and to allow a good trade-off between spatial resolution and computation time.

For the present analysis, we wish to use events that occurred throughout the time fluid was being injected. We wanted to limit the number of events to reduce computation time while still getting enough ray coverage to allow us to reliably determine a reservoir image. Choosing events on the basis of RMS residual calculated after locating the earthquakes using a homogeneous velocity model may not be a reliable event-selection method since large residuals for some events may indicate the need for a heterogeneous velocity model. The following procedure was used to select only those events that we considered to have the most reliable locations. First, we selected only events that had a total of at least six arrival-time picks. We located each event $n+1$ times where n is the number of arrival-time picks for the event. Locations were determined first using all the picks and then using all subsets of $(n-1)$ picks. The $n+1$ locations for each event were compared and if they all fell within 100 m of each other, we considered the location to be well-determined. This procedure resulted in a data set consisting of 3886 events. The locations of these events found using the single-event location procedure described by House (1987) are shown in Fig. 1c.

3. Travel-time tomography

In our tomography study, we assume that the region under investigation was relatively homogeneous rock prior to the initiation of injection and that all spatial variations in velocity are caused by the injection process. Thus, we define a region of investigation to encompass a zone surrounding the injection interval and consider that seismic rays encounter no velocity anomalies once they travel outside this region.

3.1. Method using second difference regularization

In the travel-time tomography analysis conducted by Block et al. (1994), the 3D velocity structure for both P- and S-waves and the locations of the microearthquakes were determined. The inversion grid was a node-based model with velocities specified at nodes and linearly interpolated between nodes. The ray-tracing routine of Um and Thurber (1987) was used with slight modifications introduced to improve reliability for rays passing through zones with large velocity contrasts (Block, 1991). The accuracy of the modified ray-tracing code was discussed by Block (1991), who showed that the method is reliable to better than 0.1% of the total travel time for paths having lengths of 500 m through structures having up to 30% variation in velocity at adjacent nodes. The method of parameter separation was used to decouple the location calculation portion of the problem from the inversion for velocity structure while still maintaining the formalism of a simultaneous inversion (Pavlis and Booker, 1980). Block et al. (1994) introduced several constraints to reduce the inherent nonuniqueness of the velocity determination. In addition to finding a model that gave the best RMS fit to the travel-time data (square root of sum of squared difference between data and model predictions of travel times), they added a constraint that spatially smoothed the velocity model, as well as a penalty function that favored a decrease in the velocities compared to the starting model. Thus, they minimized:

$$\sum_{\text{P, S Arrivals}} (t_{\text{m}} - t_{\text{i}})^2 + \left(\lambda \sum_{\text{Velocity nodes}} (\delta^2 v) \right) + \left(\beta \sum_{\text{nodes with } v > v_0} (v - v_0) \right) \quad (1)$$

where t_{m} is the measured travel time for one micro-

earthquake at one station, t_i is the predicted travel time, λ, β are empirically determined Lagrangian multipliers, $\delta^2 v$ is a local measure of smoothness of the 3D velocity model in the vicinity of a grid point in the model, v is the velocity at a grid point in the model, and v_0 is the velocity of the region prior to the start of injection. The Lagrangian multipliers are chosen to provide a reasonable trade-off between desired characteristics of the model and the fit to the data, as discussed below.

The constraints were imposed to stabilize the inversion. The physical basis of each constraint was considered reasonable. The smoothness constraint was justified by the assumption that the fluid injection does not cause rapid spatial variations in seismic velocity. The constraint that the velocity decreases was imposed since it is assumed that the injection process results in the introduction of fluid-filled fractures in the rock, which are well-known to reduce seismic velocities (Nur and Simmons, 1989).

Block et al. (1994) showed images obtained for the first portion of the hydraulic fracturing operation. It was considered to be unreasonable to include data from later in the experiment in the same inversion since the velocity structure was presumed to change with time so that the structure appropriate for early events would be different from the one appropriate for later events. The main objective of introducing the time-varying approach is to allow us to use more microearthquakes in the inversion for velocity structure.

3.2. Incorporating time variations of velocity structure in tomographic analysis

We would like to extract as much reliable information about the temporal change in velocity structure during the fluid injection as possible. Information about where and when velocity changes occur would be extremely useful for modeling the fluid injection process and would provide valuable information about the fracture system. However, the locations of microearthquakes change during the injection so that the regions of the reservoir that are sampled by rays traveling between sources and receivers also change. Comparing the tomograms derived from microearthquakes that occurred during two time intervals is not a reliable way to detect temporal change in the reservoir since the spatial resolution of the tomograms will be different. The difference in resolution results from the different distribution of the microearthquakes. Thus, we seek some other method to evaluate the temporal change in velocity of the reservoir.

Figs. 2–4 show that the volume of rock that is seismically active increases during the period of injection. They also show that the seismically active volume increases approximately linearly with the injected fluid volume. Thus, it is reasonable to assume that a given element of rock absorbs approximately the same amount of fluid in some period of time after the fluid front reaches it no matter where in the reservoir it is located. We therefore assume that the velocity of a region is initially the intrinsic rock velocity and that it changes to some other velocity only after a given number of microearthquakes occur within it.

We divide the region of investigation into blocks having dimensions of 50 m in the east–west direction and 100 m in the north–south and depth directions. Rays from the initial portion of the experiment propagate through the region at the background velocity. After five microearthquakes have occurred in the region, rays propagate through it at some velocity that is found by the inversion. We damp the velocity inversion slightly by assuming that the velocities of all altered regions are the same unless the data strongly indicate that they are different. We introduce this damping with a regularization parameter. We also used the constraint introduced by Block et al. (1994) to favor models having velocities lower than the background velocities. Thus, we seek to minimize:

$$\sum_{\text{P, S Arrivals}} (t_m - t_i)^2 + \left(\lambda \sum_{\text{Velocity nodes}} |v - v_{av}| \right) + \left(\beta \sum_{\text{nodes with } v > v_0} (v - v_0) \right) \quad (2)$$

where v_{av} is the average of the velocity of all nodes that have altered velocity. In this inversion, the requirement that a region surrounding a node must contain a number of microearthquakes before its velocity is allowed to vary will mean that the velocities at most nodes whose velocities are determined by the inversion are relatively well resolved. Thus, the

regularization parameter λ can be chosen to be small so that the effects of the constraint favoring models with similar velocities in regions having altered velocity can be made relatively weak. The procedure introduced here also gives better spatial resolution of the velocity model than when using the second difference regularization since the second difference approach tends to smear anomalies and produce artifacts in the form of side-lobes around strong velocity anomalies.

3.3. Test of the temporal variation approach

To test the temporal variation approach to travel-time tomography and to investigate the resolution of the method, synthetic data were generated and inverted using various values of λ in Eq. 2. Locations of microearthquakes were taken to be those of the 3886 microearthquakes shown in Fig. 1c. Station geometry was chosen to be identical to that of the real data set (Fig. 1a). Synthetic data were generated for a velocity model that was constant everywhere except for one node located near the injection interval. Fig. 5 shows a horizontal slice through the P- and S-wave velocity models. The depth of the slice is 3500 m beneath the surface, which was the depth of the node whose velocity was different from the background. In this case, the velocity was allowed to change after five microearthquakes had occurred in a 50 m by 100 m by 100 m block surrounding the node. The S-wave velocity was lowered proportionally more than the P-wave velocity under the assumption that fluid-filled cracks have a greater impact on S- than on P-wave velocity (Block et al., 1994). Gaussian-distributed random noise with a mean of zero and standard deviations that differ for each station and seismic phase were added to the travel times predicted by ray-tracing through the model. The standard deviations were equal to our estimate of picking error for each station as discussed in Section 2. Larger noise was added to the S-wave arrivals than to the P-wave arrivals to be consistent with the estimated picking error in the real arrival-time picks.

The initial velocity model was chosen to be a homogeneous structure. Initial microearthquake locations were determined by a single-event location procedure using the synthetic arrival-time data and a homogeneous velocity structure. The tomography method successfully recovered the location of the low-velocity zone in the S-wave structure. The velocity found at that location, however, was greater than the velocity in the model used to generate the synthetic data. The P-wave velocities are not well resolved. The poor quality of the P-wave tomogram will be discussed below. We investigated the trade-

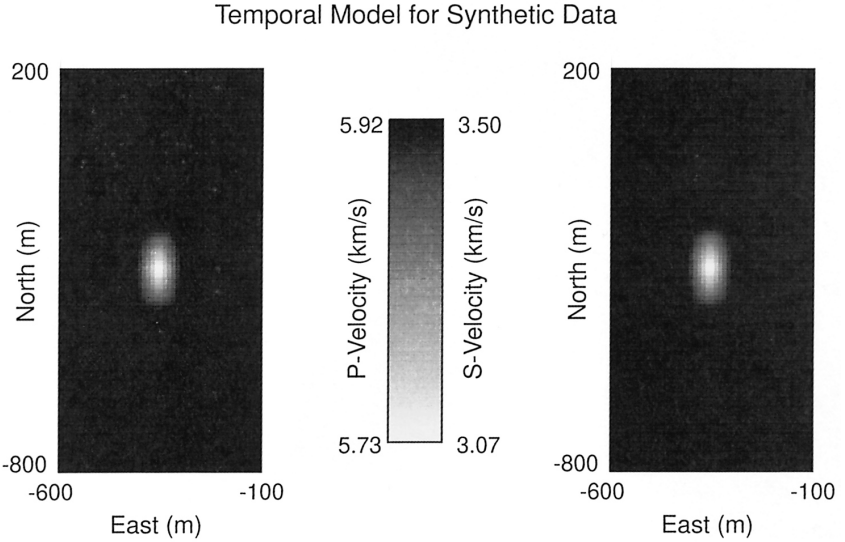

Fig. 5. Horizontal slice through velocity model used to generate synthetic travel-time data for testing the inversion algorithm. Depth of slice is 3500 m, near the center of the injection zone. The only velocity anomaly in the model was centered at this depth.

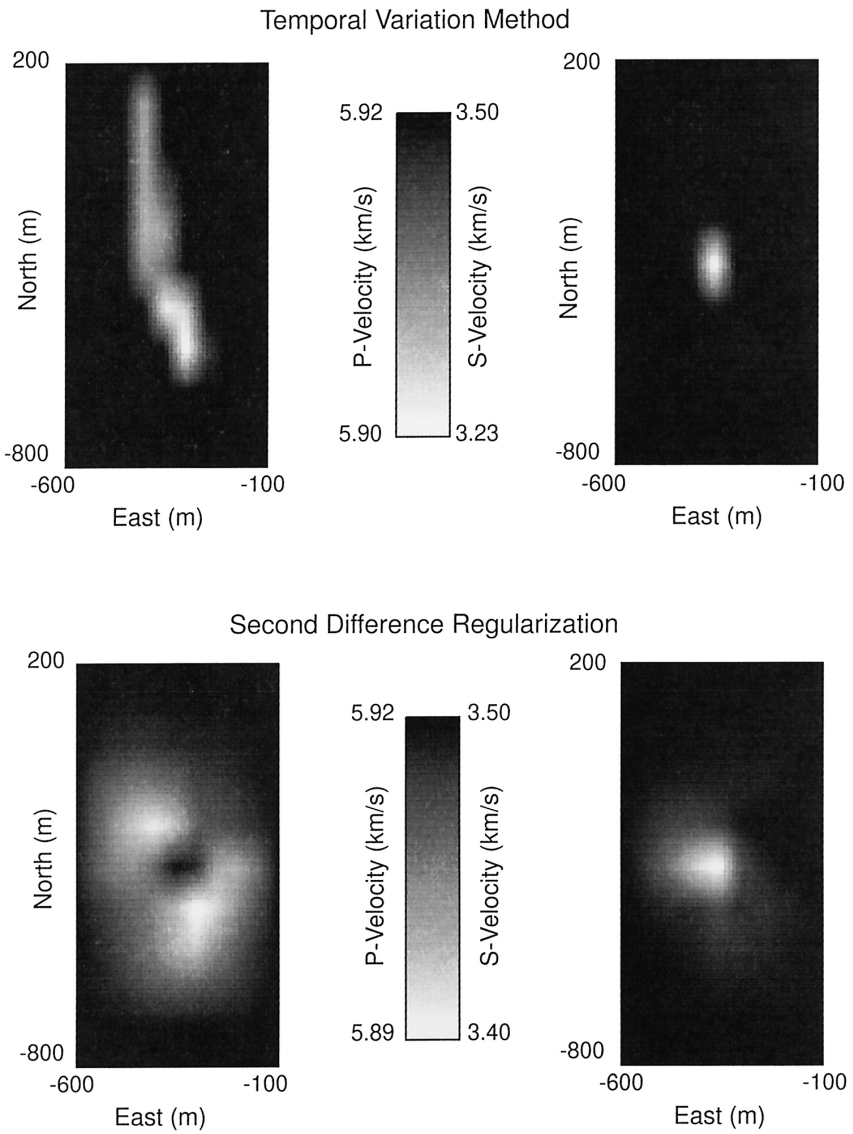

Fig. 6. Result of inverting for velocity structure using synthetic data generated for the model in Fig. 5 and microearthquakes in Fig. 1c. Upper two panels are horizontal slices through P (left) and S (right) wave models obtained at 3500 m depth using the time-varying scheme; the lower two panels are models obtained using second difference regularization scheme.

offs between the minimum S-wave velocity at the location of the velocity anomaly and the RMS residual for various values of λ. For small values of λ we found that the RMS residual and the minimum S-velocity were relatively insensitive to λ. As the regularization parameter increased, the RMS residual increased and the velocity anomaly found by the inversion increased in spatial extent and the velocity increased. We chose the largest λ that fell within the range where RMS was insensitive to the value chosen. This approach was taken to balance the trade-off between our desire to have the minimum impact on the image while reducing the effects of noise or poor resolution.

Fig. 6 shows slices through the P- and S-velocity models found by inversion of the synthetic data using

both the second difference regularization method of Block et al. (1994) and the time-varying approach. The slices show the same depth as those in Fig. 5. The regularization parameter λ was chosen to be 4 for the method of Block et al. (1994) and 30 for the time-varying approach. The value of 4 was chosen for the method of Block et al. (1994) to be consistent with their results. Fig. 6 shows that the second difference regularization method smears the anomaly over a broader region than does the time-varying approach.

As found by Block et al. (1994), the P-wave tomogram is poor in quality compared to the S-wave tomogram. They explained the difference in image quality as resulting from the relatively smaller travel-time anomalies for P-waves compared to and S-waves that are produced by fluid-filled fractures. Block et al. (1994) show that the estimated uncertainty of the S-wave arrival times, while larger than that of the P-wave arrival times, is still smaller than the travel-time anomalies caused by fluid-filled fractures while the uncertainty of the P-wave arrival times is larger than the anomalies caused by the fractures. P-wave tomograms are therefore considered unreliable and we will not show the P-wave tomograms from the analysis of real data. Block et al. (1994) argued that there is some useful information in the P-tomograms since they were not able to achieve a meaningful reduction in travel-time residuals if P-velocities were held constant. They suggested using fewer nodes for the P-model as a way to improve the reliability of the result. They did not do this nor did we.

4. Results and discussion

Fig. 7 shows the S-wave tomograms obtained for the depth slice at 3500 m obtained by the time-varying and the second difference regularization approaches. The tomogram obtained by the second difference approach using data from the entire injection is dramatically different from the one obtained by Block et al. (1994) which used data from only early in the injection. Nevertheless, there are similarities between the tomogram obtained with the time-varying approach and the one in Block et al. (1994). In Fig. 7, the anomalies in the second difference tomogram are spread throughout the region imaged and do not have a direct relation to the locations of the seismic events, shown in Fig. 8. In contrast, the time-varying tomogram shows a clear low-velocity anomaly located near the injection zone. There is also a small anomaly located to the southeast of the injection zone at the same depth. Dashed lines in Fig. 8 show two linear trending zones of microearthquake locations that continue through the zone with

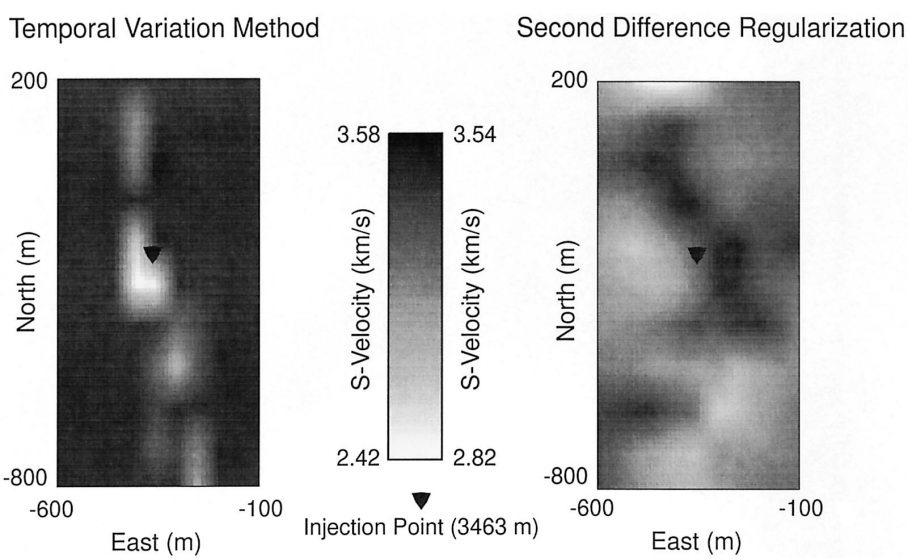

Fig. 7. Horizontal slices at 3500 m depth of S-wave velocity models obtained using field data and time-varying scheme (left) and second difference regularization scheme (right).

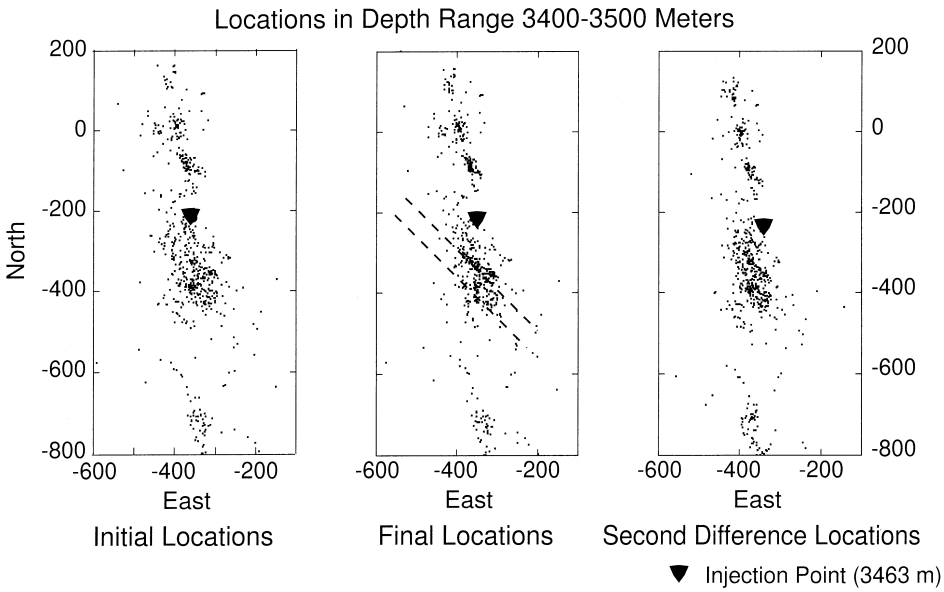

Fig. 8. Locations of microearthquakes within depth range 3400–3500 m found using homogeneous velocity model and single-event location scheme (left), time-varying tomography scheme (middle), and second difference regularization scheme (right). Dashed lines show alignments of locations along trends that pass through a zone having background velocity.

background velocity between these two low-velocity zones (Fig. 7).

The locations of the microearthquakes found by the time-variation method moved an average of 21 m from their starting locations. Those starting locations were found using a homogeneous velocity structure. The mean depth of the microearthquake locations from the time-varying tomography inversion decreased an average of 15 m from the initial locations. The average change in location in the horizontal plane was much smaller than in the vertical. The decrease in the mean depth agrees with the results found by Block et al. (1994). Events shallower than the injection zone changed little in

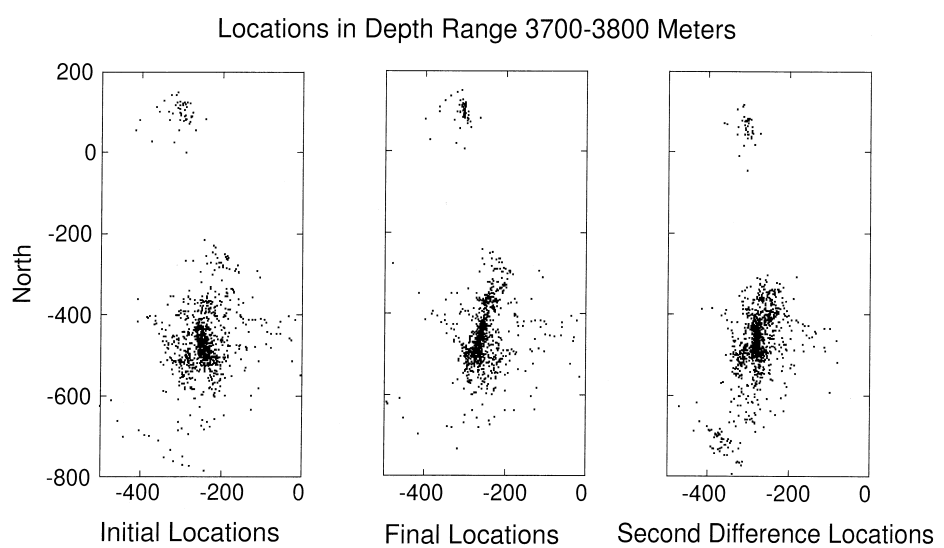

Fig. 9. Same as Fig. 8 except depth range is 3700–3800 m.

depth but events below the injection zone generally moved slightly shallower. This can be explained by the presence of the low-velocity zone located near the injection zone that slows the rays along paths between deeper microearthquakes and the stations. When the microearthquakes are located using a homogeneous velocity model, the event locations are moved deeper because of the higher velocity.

The mean RMS travel-time residual decreases about 7% from the time-varying analysis. This compares with a 11–15% decrease of RMS residual found by Block et al. (1994) for their time-limited data set. The smaller reduction in RMS residual for the temporal variation method is consistent with a greatly reduced number of free parameters in the inversion since nodes that are not near microearthquakes keep the background velocity. In the second difference approach, the velocities of all nodes are allowed to vary. For the time-varying approach, velocities varied in a total of 139 nodes, which is less than 10% of the total number of nodes whose velocities varied in the second difference scheme.

Inspection of Figs. 8 and 9 shows that there is more structure in the pattern of microearthquake locations found by the time-varying tomography than in the initial location data set. Several linear alignments of locations can be seen and some small clusters of events appear to form tighter clusters in the locations determined using the time-varying approach compared to the locations using the homogeneous structure or the structure derived from the second difference tomography scheme. On average, locations from the time-varying method fall about 10 m closer to the injection zone than the locations from the homogeneous velocity model. However, there is an aseismic zone surrounding the injection zone (located at north 218, and east −356) that is larger in the plot showing locations found using the time-varying velocity structure (middle of Fig. 8). The radius of this zone grows from 10 to 30 m when locations are determined using the heterogeneous structure found by the time-varying analysis.

5. Conclusions

We have presented a method to perform tomography analysis of microearthquake data collected during hydraulic fracturing when it can be assumed that the velocity structure changes with time. The method relies on a simple assumption about how the velocity structure should change with time, which is justified by observations of how the size of the seismically active volume changes with time. The method allows the use of data from throughout a hydraulic fracturing operation, and results in an improved image of the velocity anomalies that result from fracturing of the rock. The spatial pattern of microearthquake locations computed by the method has more structure than appears in the pattern of locations found using a homogeneous velocity structure or using a structure found from a tomography scheme that allows no temporal change. The pattern of locations found by the time-varying tomography method shows a good correlation with the velocity structure. The more spatially-focused pattern of locations is evidence that the method is an improvement over the assumptions that the velocity structure does not change with time.

The method provides a consistent way to use data from throughout a long hydraulic fracturing operation where it is reasonable to consider that the velocities change with time. Use of data from throughout the experiment allows a larger set of microearthquakes that satisfy rigid selection criteria to be used, which should also result in an image with greater spatial resolution compared to what can be obtained with other methods. This image and the improved microearthquake locations can provide valuable information about where and how fluid permeates in rock during the hydrofracturing process.

Acknowledgements

We thank Lisa Block for providing her tomography code that formed the foundation of this study. Comments from Cezar Trifu and two anonymous reviewers helped to improve the presentation of this work. Support for this project came from the Department of Energy Office of Basic Energy Sciences through Bill Luth. Bill's support of our work is gratefully appreciated. This work was funded by DOE Contract W-7405-ENG36 from the U.S. Department of Energy to Los Alamos National Laboratory.

References

Aki, K., Fehler, M., Aamodt, L., Albright, J., Potter, R., Pearson, C., Tester, J., 1982. Interpretation of seismic data from hydraulic fracturing experiments at the Fenton Hill, New Mexico, Hot Dry Rock geothermal energy site. J. Geophys. Res. 87, 936–944.

Block, L., 1991. Joint hypocenter–velocity inversion of local earthquake arrival time data in two geothermal regions. Sc.D. Thesis, Mass. Inst. Technol.

Block, L., Cheng, C.H., Fehler, M., Phillips, W.S., 1994. Seismic imaging using microearthquakes induced by hydraulic fracturing. Geophysics 59, 102–112.

Duchane, D., 1994. Geothermal Energy. In: Kirk-Othmer Encyclopedia of Chemical Technology (4th ed.), Vol. 12. John Wiley, New York.

Fehler, M., 1981. Changes in P wave velocity during operation of a hot dry rock geothermal system. J. Geophys. Res. 86, 295–298.

Fehler, M., 1989. Stress-control of seismicity patterns observed during hydraulic fracturing experiments at the Fenton Hill Hot Dry Rock Geothermal Energy Site, New Mexico. Int. J. Rock Mech. Min. Sci. Geomech. Abstr. 26, 211–219.

Harlow, F., Pracht, W., 1972. A theoretical study of geothermal energy extraction. J. Geophys. Res. 77, 7038–7048.

House, L., 1987. Locating microearthquakes induced by hydraulic fracturing in crystalline rock. Geophys. Res. Lett. 14, 919–921.

Michelini, A., McEvilly, T., 1991. Seismological studies at Parkfield, I. Simultaneous inversion for velocity structure and hypocenters using cubic B-splines parameterization. Bull. Seismol. Soc. Am. 81, 624–652.

Nolet, G. (Ed.), 1987. Seismic Tomography. D. Reidel, Boston. MA.

Nur, A., Simmons, G., 1989. The effect of saturation on velocity in low porosity rocks. Earth Planet. Sci. Lett. 7, 183–193.

Paulsson, B., Smith, M.E., Tucker, K.E., Fairborn, J.W., 1992. Characterization of a steamed oil recovery using cross-well seismology. Leading Edge 11 (7), 24–32.

Pavlis, G.L., Booker, J., 1980. The mixed discrete–continuous inverse problem: application to the simultaneous determination of earthquake hypocenters and velocity structure. J. Geophys. Res. 85, 4801–4810.

Pearson, C., Fehler, M., Albright, J., 1983. Changes in compressional and shear wave velocities and dynamic moduli during operation of a hot dry rock geothermal energy system. J. Geophys. Res. 88, 3468–3475.

Phillips, W.S., House, L., Fehler, M., 1997. Detailed joint structure in a geothermal reservoir from studies of induced microearthquake clusters. J. Geophys. Res. 102, 11745–11763.

Trice, R., Warren, N., 1977. Preliminary study on the correlation of acoustic velocity and permeability in two granodiorites from the Los Alamos Fenton Hill deep borehole, GT-2, near the Valles Caldera, NM. Rep. LA-6851-MS, Los Alamos Sci. Lab., Los Alamos, NM.

Um, J., Thurber, C., 1987. A fast algorithm for two-point seismic ray tracing. Bull. Seismol. Soc. Am. 77, 972–986.

Weiland, C., Steck, L., Dawson, P., Korneev, V., 1995. Nonlinear teleseismic tomography at Long Valley Caldera, using 3-dimensional minimum travel-time ray-tracing. J. Geophys. Res. 100, 20379–20390.